Received: 26 February 2024 | Accepted: 12 July 2024

DOI: 10.1002/bem.22522

RESEARCH ARTICLE

BioEM WILEY

Nonlinearities and timescales in neural models of temporal interference stimulation

Tom Plovie MSc[1] | **Ruben Schoeters PhD**[1] | **Thomas Tarnaud PhD**[1,2] | **Wout Joseph PhD**[1] | **Emmeric Tanghe PhD**[1]

[1]WAVES, Department of Information Technology, Ghent University, Ghent, Belgium

[2]4Brain, Department of Head and Skin, Ghent University, Ghent, Belgium

Correspondence

Tom Plovie, MSc, WAVES, Department of Information Technology, Ghent University, Ghent, Belgium.
Email: tom.plovie@UGent.be

Funding information

Fonds Wetenschappelijk Onderzoek, Grant/Award Numbers: 11E4520N, 1230222N, G019121N

Abstract

In temporal interference (TI) stimulation, neuronal cells react to two interfering sinusoidal electric fields with a slightly different frequency (f_1, f_2 in the range of about 1–4 kHz, $|f_1 - f_2|$ in the range of about 1–100 Hz). It has been previously observed that for the same input intensity, the neurons do not react to a purely sinusoidal signal at f_1 or f_2. This study seeks a better understanding of the largely unknown mechanisms underlying TI neuromodulation. To this end, single-compartment models are used to simulate computationally the response of neurons to the sinusoidal and TI waveform. This study compares five different neuron models: Hodgkin-Huxley (HH), Frankenhaeuser–Huxley (FH), along with leaky, exponential, and adaptive-exponential integrate-and-fire (IF). It was found that IF models do not entirely reflect the experimental behavior while the HH and FH model did qualitatively replicate the observed neural responses. Changing the time constants and steady state values of the ion gates in the FH model alters the response to both the sinusoidal and TI signal, possibly reducing the firing threshold of the sinusoidal input below that of the TI input. The results show that in the modified (simplified) model, TI stimulation is not qualitatively impacted by nonlinearities in the current–voltage relation. In contrast, ion channels have a significant impact on the neuronal response. This paper offers insights into neuronal biophysics and computational models of TI stimulation.

KEYWORDS

computational neuron models, ion gates, point neurons

1 | INTRODUCTION

Nowadays, many applications for brain stimulation exist. One of these applications is deep brain stimulation (DBS) that was mainly developed to treat movement disorders, such as Parkinson's disease (PD). However, it has an important disadvantage: it is invasive and can cause complications (e.g., bleeding in the brain, stroke, infection) (Aum & Tierney, 2018). Noninvasive brain stimulation techniques exist like transcranial direct current stimulation (tDCS), transcranial alternating current stimulation (tACS), and transcranial magnetic stimulation (TMS), but none of these is able to reach subcortical regions with adequate spatial resolution. Because of this, a new technique is being developed named temporal interference (TI) stimulation. With this technique, two sinusoidal electric fields, oscillating at a high but slightly different frequency, are applied to the brain by two cathode–anode pairs. These electrode pairs can be placed on the scalp or on the cortical surface. At the place where the oscillating fields interfere, an amplitude-modulated signal is created. This is illustrated in Figure 1. The frequency at which the envelope repeats is called the beat frequency. Grossman et al. (2017, 2018) has found from experiments on mice that cortical and hippocampal neurons respond to this interference pattern but not to the constituent sinusoids separately. Moreover, the neurons are entrained to the beat frequency, meaning that an action potential (AP) is elicited at every beat. Therefore, TI stimulation is a noninvasive alternative to the

conventional, invasive DBS techniques. Other experiments in mice have shown that it is possible to cause eye movements at the beat frequency of the TI signal (Song et al., 2021), confirming the importance of the beat frequency and indicating that the neurons are entrained to the beat frequency. It should be noted that TI stimulation is not only used in the brain. It was shown in rats that TI stimulation can activate spinal motor neurons in the neck to restore breathing after opioid overdose. Again it was shown that a single sine waveform is not able to cause stimulation (Sunshine et al., 2021). Furthermore, TI has been studied for retinal stimulation (Su et al., 2021). Typical frequencies that are used in in vivo studies are in the range of 1–5 kHz with beat frequencies of 1–100 Hz. Furthermore, instead of using electrodes to create an amplitude modulated electric field inside the brain, it is also possible to use TMS coils, creating a magnetic field and inducing an electric field. It is possible to achieve a TI waveform by using the same technique of applying multiple frequencies to the brain (Sorkhabi et al., 2020; Xin et al., 2021). Khalifa et al. (2023) proposed a slightly different method using electromagnetic solenoids instead of TMS coils generating the magnetic fields. Another slight adaptation to the technique is pulse-width modulated TI, where square waves with a different frequency temporally interfere (Luff, Dzialecka, et al., 2024; Missey et al., 2021). Although promising, there are still some limitations to overcome before TI stimulation can be used for humans and can replace conventional DBS. A first limitation is that the mechanism in the neuron that allows this type of stimulation is unknown. It is thus very hard to predict how different neuron types will react to the stimulation and thus how exactly the human brain responds to TI stimulation. A second limitation is that the technique has only been extensively tested on rodents, while very few studies are performed with experiments on humans. Piao et al. (2022) performed a safety evaluation in 38 healthy adults and no adverse effects were seen. However, the stimulation target was located in the cortex. Safety recommendations based on the current knowledge of TI stimulation and other, similar techniques (DBS, tACS, and tDCS) have been reported by Cassarà et al. (2022). One study reports TI stimulation of the human hippocampus with improved episodic memory accuracy as a result (Violante et al., 2022). Another study used TI stimulation to show an increase in activity in the striatum and in its functional brain network. This resulted in a better performance in a motor learning task, with a prominent improvement for healthy older subjects (Wessel et al., 2022). Furthermore, Vassiliadis et al. (2024) showed the importance of the striatum in reinforcement learning processes via the use of TI stimulation.

To get more insight into the electric field distribution of TI stimulation in the human brain, finite element method (FEM) simulations have been performed. In these studies, TI stimulation has been compared to a conventional technique like tACS. This showed that

Highlights

- The mechanism of TI stimulation is influenced by nonlinearities of ion channels.
- Goldman–Hodgkin–Katz nonlinearity is not required for modeling TI stimulation.
- An optimal beat frequency can be chosen to maximize the working of TI stimulation on the level of ion channels.

when the same electric field strength is achieved inside the focus, TI induces a smaller maximal electric field outside this focus than tACS (von Conta & Kasten, 2021). Both the electric field amplitude and the modulation index are relevant for stimulation. The modulation index influences the activation threshold, while the amplitude then determines whether activation occurs. In contrast to the traditional DBS technique, it is easier to steer the stimulation site with TI stimulation. This can be done by changing the electrode positions or by adjusting the relative amplitudes of the current at the different electrode pairs (Gomez-Tames et al., 2021; Rampersad et al., 2019; von Conta & Kasten, 2021). With these degrees of freedom, it is

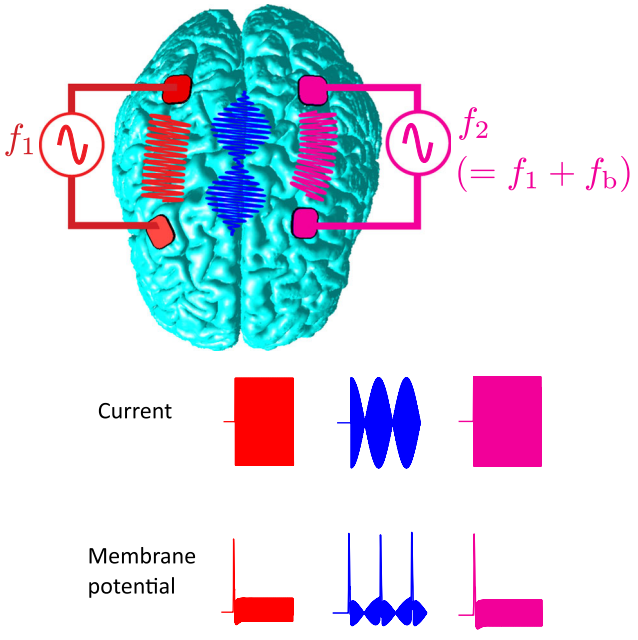

FIGURE 1 Schematic illustration of the concept of TI-DBS in the MIDA brain (Iacono et al., 2015). The red and pink electric field oscillate at a different frequency. At the place where they temporally interfere, the blue amplitude modulated signal is created. TI electrodes could be placed on the scalp or on the cortical surface. The corresponding waveforms in the ideal situation where the TI signal causes spikes and the pure sinusoids do not (besides the initial AP) are shown on the bottom.

possible to find the optimal electrode positions for focal targeting. This optimal electrode positioning is very subject-specific. With the same electrode positioning, high variations are possible in the simulated electric fields for different people (von Conta & Kasten, 2021). Huang and Parra (2019) argue that it is possible to achieve sufficiently high electric fields in deep brain regions using tACS. To achieve this, the electrode positioning becomes more important because it makes use of the cerebrospinal fluid as a conductor for the electric field. It is thus even more challenging to obtain a patient-specific electrode position. They do mention that the focality is still worse with this technique than with TI stimulation (Huang & Parra, 2019). The focality in TI stimulation is in the centimeter range (Huang et al., 2020). Lee et al. (2022) proposed epidural TI stimulation, where the electrodes are placed under the skull, in order to avoid stimulation in cortical regions. They validated their FEM simulations with phantom experiments. Furthermore, the feasibility of TI stimulation in humans is investigated by Acerbo et al. (2022) with the use of mice models and human cadavers in combination with simulations for the optimal electrode positioning.

It was found in silico and in vivo that increasing the carrier frequency of the TI signal increases the threshold of the input needed to cause stimulation. In in vivo studies by Grossman et al. (2017) and Gomez-Tames et al. (2021), changing the beat frequency did not seem to have an influence on the threshold. Budde et al. (2023) does report a *U*-shaped threshold as a function of the beat frequency. Furthermore, it is reported that peripheral nerves do not extract the envelope of the TI signal (Budde et al., 2023). This is in contrast with the ex vivo neurons of Luff, Peach, et al. (2024), where it is seen that neurons do show a certain energy at the beat frequency in the frequency spectrum. Martinez et al. (2023) showed in an ex vivo study that the activation thresholds for both a sinusoidal and TI signal are cell-specific. Moreover, the individual exhibition of TI is altered when put in a neuronal network.

On the other hand, in silico, Mirzakhalili et al. (2020) and Howell and McIntyre (2021) do mention the importance of the beat frequency for the activation threshold. Furthermore, Plovie et al. (2022) showed that for a reduced Hodgkin-Huxley (HH) model, the excitation threshold changes with both carrier and beat frequency. To model TI stimulation, it was found that integrate-and-fire (IF)-neurons are not sufficient to reproduce the experimental behavior on single neuron level (Cao et al., 2020). However, when IF-neurons are placed in a network and $GABA_b$ postsynaptic inhibition is included, the computational results were in line with experimental observations of TI stimulation in hippocampal slices (Esmaeilpour et al., 2021). Further on, for point neurons, it is possible to have neurons exhibiting TI stimulation when using the FitzHugh–Nagumo model or the HH model. It was also seen that not all mammalian neurons exhibit TI (Cao et al., 2020; Cao & Grover, 2018). Howell and McIntyre (2021) argues that because of the large dimensions of a human head, TI stimulation seems infeasible. However, it is suggested that subthreshold TI stimulation can be used to synchronize the firing of neurons to the TI signal. Next to the immediate effect on the neuron, TI stimulation could also, like other electrical stimulation methods, impact the plasticity and the interconnectivity of neurons (Howell & McIntyre, 2021). Up to now, it was said that high-frequency signals do not cause stimulation. This is not entirely true: there are actually multiple ways for a neuron to respond to a high-frequency signal. There can be for example one AP at the signal onset, continuous firing or depolarization block. It may be impossible to stimulate the deep regions of the brain without also causing a conduction block in other parts of the brain (Mirzakhalili et al., 2020). This conduction block occurs at higher input intensities and could lead to an upper limit for the use of TI stimulation (Grossman et al., 2017). The conduction block was also seen in Wang et al. (2023), with morphologically realistic neuron models at amplitudes that were an order of magnitude larger than the amplitude for activation. This again shows the difficulty with off-target regions during TI stimulation (Wang et al., 2023).

Regarding the underlying mechanism at the neuron level that enables this stimulation type, one of the earliest hypotheses was that TI stimulation can be explained in terms of the intrinsic low-pass filter property of a neuron together with a nonlinear component. For example, in the HH framework, the cell membrane is modeled by a parallel RC circuit, thus implementing a low-pass filter when driven by a current source (Hodgkin & Huxley, 1952). Here, a first nonlinearity is introduced in the time-dependent resistor, through the ion channel dynamics. Indeed, the channel opening and closing rate functions depend nonlinearly on the membrane potential. Furthermore, subsequent work has generalized the Ohmic current–voltage relation in the HH model to account for the nonlinear distribution of electrolyte concentration along the ion channel (Frankenhaeuser & Huxley, 1964). The resulting Goldman–Hodgkin–Katz (GHK) current–voltage relation introduces a second nonlinearity to the equation set. Because of the low-pass filter property, the neuron cannot react to the high-frequency oscillations and therefore responds to the low-frequency envelope of the TI signal (Grossman et al., 2017, 2018).

It is clear that the low-pass filter property cannot be the single explanation because with only the properties of a low pass filter, the envelope could not be extracted by the neuron and it would not respond to the beat frequency, meaning it would not contain spectral content on the beat frequency. This is because the TI waveform, as a sum of two high-frequency sines, does not contain spectral content at the beat frequency. As a result, a pure low-pass filter will not give spectral components at the beat frequency. Alternatively, by

first rectifying the signal and then low-pass filtering, which is equivalent to an envelope detection of the TI signal, the beat frequency is extracted. According to Mirzakhalili et al. (2020), a rectification process is needed in order to have a response to the TI-stimulus. This rectification could come from a nonlinear response of the neuron as stated by Mirzakhalili et al. (2020). However, the neuronal membrane cannot be a perfect demodulator because high-frequency oscillations (i.e., the frequencies of the constituent sines) can still be found in the membrane potential response. Because it is not a perfect rectification, it is called quasi-rectification (Cao & Grover, 2018; Mirzakhalili et al., 2020). The exact neuronal requirements for the rectification are unclear. According to Luff, Peach, et al. (2024), however, the signal mixing properties of the neuron could explain the mechanism of TI stimulation.

The first finding of this paper is the demonstration that the nonlinearity of the GHK equation in the Frankenhaeuser–Huxley (FH) model is not strictly required to show the effect of TI stimulation found in Grossman et al. (2018). Consequently, our model results indicate that envelope detection can be realized at the membrane level through the nonlinearity intrinsic to ion channel gating. A second finding is the required aspects in a computational neuron model to show the effect of TI stimulation, following from the comparison of biologically inspired models (FH and HH) and different IF models. The third novel aspect is a thorough investigation of the different influences of both the time constants and the steady-state parameters of the gates to obtain a biophysical explanation of the neuronal response to TI stimulation in the first place. It was already mentioned by Mirzakhalili et al. (2020) and Cao et al. (2020) that the time constants influence the excitation threshold. In this study, this is investigated in more detail. This is a step towards understanding the bigger picture of the mechanism of TI stimulation in morphological realistic neurons.

2 | METHODS

2.1 | Neuron models

In this study, single-compartment models are used. This means that the morphology of the neuron is not taken into account. This can be justified as the idea is to investigate the influence of nonlinearities on the neuronal response to create APs to sinusoidal signals and TI signals. The axial resistive coupling of neuronal compartments does not add any nonlinearities and is thus not thought to have a big influence on the underlying mechanism of TI stimulation.

The five existing models that are used are the HH (Hodgkin & Huxley, 1952), FH (Frankenhaeuser & Huxley, 1964), leaky integrate-and-fire model (LIF), exponential integrate-and-fire (EIF) and the adaptive and exponential integrate-and-fire (AdEx) model. The first two are described by the following equations:

$$C_{\mathrm{M}}\frac{dV}{dt} = I_{\mathrm{e}} - \left(I_{\mathrm{l}} + \sum_{X} I_{\mathrm{X}}\right), \tag{1}$$

$$I_{\mathrm{l}} = g_l(V - E_l), \tag{2}$$

$$\tau_{\mathrm{x}}(V)\frac{dx}{dt} = x_\infty(V) - x, \tag{3}$$

$$\tau_{\mathrm{x}}(V) = \frac{1}{\alpha_x(V) + \beta_x(V)} \tag{4}$$

$$x_\infty(V) = \frac{\alpha_x(V)}{\alpha_x(V) + \beta_x(V)} \tag{5}$$

where C_{M} is the membrane capacitance, V is the membrane potential, I_{e} is the input current, I_{l} is the leak current (with g_l and E_l being the leak conductance and the reversal potential of the leak current) and I_{X} are the currents linked to voltage-dependent gates, where X can be Na, K, or p (sodium, potassium and a nonspecific current, respectively). According Frankenhaeuser and Huxley (1964), the nonspecific p-current is largely consisting of sodium ions and possibly other ions such as calcium. The values for all of the constants are taken from Hodgkin and Huxley (1952) and Frankenhaeuser and Huxley (1964) and are summarized in Table 1. In Equation (3), x can be m, h, n, or p. These are the open probabilities of the respective gates. p is only used in the FH-model. $\tau_x(V)$ and $x_\infty(V)$ are the time constant and the steady-state value characterizing the gates. $\tau_x(V)$ and $x_\infty(V)$ are related to the opening and closing rates ($\alpha_x(V)$ and $\beta_x(V)$). These are retrieved from Hodgkin and Huxley (1952) and Frankenhaeuser and Huxley (1964) and are written out in the supplementary material. For TI, I_{e} is of the form $I_{\mathrm{e}} = \frac{A}{2}(\sin(2\pi f_1 t) + \sin(2\pi f_2 t)) = A\cos(\pi f_b t)\sin(2\pi f_c t)$, where f_b is the beat frequency and f_c is the carrier frequency. The ion currents of the FH-model, implemented as current densities, are described by:

$$I_{\mathrm{Na}} = m^2 h P_{\mathrm{Na}} \frac{VF^2}{R_{\mathrm{g}}T} \frac{[\mathrm{Na}]_o - [\mathrm{Na}]_i \exp\left(\frac{VF}{R_{\mathrm{g}}T}\right)}{1 - \exp\left(\frac{VF}{R_{\mathrm{g}}T}\right)}, \tag{6}$$

$$I_{\mathrm{K}} = n^2 P_{\mathrm{K}} \frac{VF^2}{R_{\mathrm{g}}T} \frac{[\mathrm{K}]_o - [\mathrm{K}]_i \exp\left(\frac{VF}{R_{\mathrm{g}}T}\right)}{1 - \exp\left(\frac{VF}{R_{\mathrm{g}}T}\right)}, \tag{7}$$

TABLE 1 Parameters for the Frankenhaeuser–Huxley and Hodgkin–Huxley model for 20°C and 6°C, respectively.

Frankenhaeuser–Huxley		**Hodgkin–Huxley**	
$P_{Na} = 0.008$ cm/s	$[K]_o = 2.50$ mol/cm^3	$g_{Na} = 120$ mS/cm^2	$g_l = 0.30$ mS/cm^3
$P_K = 0.00120$ cm/s	$[K]_i = 120$ mol/cm^3	$g_K = 360$ mS/cm^2	$E_l = -59.40$ mV
$P_p = 0.000540$ cm/s	$c_m = 20\,\mu$F/cm^2	$E_{Na} = 45$ mV	$c_m = 10\,\mu$F/cm^2
$[Na]_o = 114.50$ mol/cm^3	$g_l = 30.30$ mS/cm^2	$E_K = -82$ mV	
$[Na]_i = 13.740$ mol/cm^3	$E_l = -70$ mV		

$$I_p = p^2 P_p \frac{VF^2}{R_g T} \frac{[Na]_o - [Na]_i \exp\left(\frac{VF}{R_g T}\right)}{1 - \exp\left(\frac{VF}{R_g T}\right)}. \quad (8)$$

The part of Equations (6), (7), and (8) after the ion channel gate parameters (m, h, n, and p) is known as the GHK flux equation. P_{Na}, P_K, and P_p are the respective ion-specific permeabilities, F is the Faraday constant, R_g is the ideal gas constant and T is the temperature. $[Na]_o$ and $[Na]_i$ are the extracellular and intracellular concentrations of sodium, respectively. Similarly, $[K]_o$ and $[K]_i$ are the extracellular and intracellular concentrations of potassium, respectively. The ion currents of the HH-model, also implemented as current densities, are described by:

$$I_{Na} = m^3 h g_{Na} (V - E_{Na}), \quad (9)$$

$$I_K = n^4 g_K (V - E_K). \quad (10)$$

Here, g_{Na} and g_K are the ionic conductances of sodium and potassium, whereas E_{Na} and E_K are the reversal potentials of sodium and potassium, respectively. The HH- and FH-model are developed for the squid giant axon and the myelinated nerve fiber of Xenopus laevis, respectively. However, mammalian neurons function in a similar way. As the purpose of this study is to investigate the influence of the nonlinearities of the ion gates, and not to report exact activation thresholds for practical application, the models are well suited for the aims of this study.

The LIF-model is described by:

$$\tau_m \frac{dV}{dt} = RI_e - (V - V_r), \quad (11)$$

and the EIF-model is described by:

$$\tau_m \frac{dV}{dt} = RI_e - (V - V_r) - \Delta_T \exp\left(\frac{V - V_T}{\Delta_T}\right), \quad (12)$$

where τ_m is the membrane time constant, R is the membrane resistance, V_r is the resting potential, Δ_T is the slope factor that determines the sharpness of the threshold and V_T is the model intrinsic spike threshold. When the threshold V_{thresh} is reached, the potential resets to V_{reset}. Note that the LIF-model is the EIF-model in the limit of $\Delta_T \to 0$. The AdEx-model is very similar but has an additional differential equation. It is described by:

$$\tau_m \frac{dV}{dt} = RI_e - (V - V_r) - \Delta_T \exp\left(\frac{V - V_T}{\Delta_T}\right) - RW, \quad (13)$$

$$\tau_w \frac{dW}{dt} = a_0 (V - V_r) - W, \quad (14)$$

where the additional parameter a_0 determines the level of subthreshold adaptation. Again when a threshold V_{thresh} is reached, the potential is reset to V_{reset} while W is changed into $W + b_0$ (Brette & Gerstner, 2005). The parameters used for the presented results of the IF-models are given in Table 2 unless stated otherwise. The IF-models are mainly added in order to investigate which characteristics are needed in neuron models to make the neuron spike at lower inputs for a TI signal than for a sinusoidal signal.

2.2 | Neuron model extensions

To investigate the influence of the nonlinearity of the GHK-equation, two new models are constructed from the HH- and FH-model. A partly linearized version of the FH-model (FH1) is obtained by replacing the GHK-factor of Equations (6)–(8) by its first-order Taylor expansion for I_K, I_{Na}, and I_p. In Equation (15), this is shown more specifically by the transition from left to right.

$$I_X = m^\gamma h^\delta n^\epsilon p^\zeta A_X x \frac{B_X - C_X \exp(x)}{1 - \exp(x)} \leftrightarrow I_X = \left(I_X(x_{X,0}) + \frac{\partial I_X}{\partial x}(x_{X,0})(x - x_{X,0})\right), \quad (15)$$

TABLE 2 Parameters for the Integrate-and-fire (IF) models.

V_r	Membrane potential of neuron at rest	−70 mV
V_{reset}	Potential to which neuron is reset after an AP	−70 mV
V_{thresh}	Threshold to define an AP	−40 mV
R	Membrane resistance	0.5×10^6 $k\Omega$
τ_m	Time constant of membrane potential	5 ms
Δ_T	Slope factor	2 mV
V_T	Intrinsic spike threshold	−50 mV
τ_w	Time constant of adaptive current	100 ms
a_0	Subthreshold adaptation	2×10^{-9} mS
b_0	Spike-triggered adaptation	8×10^{-6} μA

where $x = \frac{F}{R_g T}V$, $A_X = P_X F$, $B_X = [X]_o$, $C_X = [X]_i$, and $x_{X,0} = \frac{F}{R_g T}V_{X,0}$. γ, δ, ϵ, and ζ are the numbers depending on the specific ion channel (see 6–10). In this transition, the gates remain the same as in the original models. The ion currents are thus still nonlinear because of the gate equations, only the part representing the GHK-equation is linearized for FH1. For the HH-model, the opposite is done. It is assumed that the HH-model is the first-order Taylor expansion of a more general model. This more general model is then of the form of Equations (6)–(8) and is called the gHH-model. In Equation (15), this corresponds to the transition from right to left. In order to obtain these new models, the right expansion points ($(V_{Na,0}, V_{K,0})$ and $(V_{Na,0}, V_{K,0}, V_{p,0})$) for this Taylor series should be found for the gHH and FH1 model, respectively. Two methods are followed to realize this, resulting in four derived models: gHHv1, FH1v1 (method 1) and gHHv2, FH1v2 (method 2).

The first method consists of calculating the reversal potentials for the ion currents (i.e., the Nernst potentials) and taking these as the expansion points. This method leads to the physiologically most relevant model. In the second method, a sweep is done over several combinations of possible Taylor expansion points. This method leads to the model that follows the voltage traces of the original model in the best way. For each set, several combinations of duration and intensity of a rectangular input signal are tested. The values for the input amplitudes are 10 uniformly distributed values between 300 and 800 $\mu A/cm^2$ for the FH-model and between 0 and 100 $\mu A/cm^2$ for the HH-model. For the stimulation duration, 10 uniformly distributed values between 0.05 and 2.00 ms are chosen for both models. For every combination, the correlation between the membrane response of the original and the new model is calculated. The correlations of the different duration–intensity combinations are averaged. The $(V_{Na,0}, V_{K,0})$-combination with the highest average correlation is chosen for the new model. For the FH1 models, it is assumed that $V_{p,0} = V_{Na,0}$.

2.3 | Ion channel parameters

To investigate the influence of the time constants, a small adaptation is made to Equation (3). A parameter k_x is introduced to scale the time constant of the gates so that

$$\tau_{x,\text{new}}(V) = k_x \tau_{x,\text{original}}(V) \quad (\text{s}), \tag{16}$$

where $\tau_{x,\text{original}}(V)$ is the time constant as a function of the membrane potential V as originally described in the FH model. Lastly the steady-state values of the gates are investigated in more detail. The equations for the steady-state values are replaced by a logistic function like Equation (17), while the original time constant equations are maintained.

$$x_\infty = \frac{1}{1 + \exp(-a(V - V_r - b))}. \tag{17}$$

The influence of the parameters a and b on the TI-effects can then be investigated. The goal of this approach is to get insight into how the behavior changes with changing parameters and not to approximate the real behavior of the neuron globally. V_r is the rest potential and is equal to −70 mV.

2.4 | Analysis of model behaviors

The analysis of the results was done based on the firing rate (FR) and the new energy metric defined below in Equation (19). To obtain the FR, first the APs need to be determined. For the IF-models, an AP is counted every time the threshold V_{thresh} is exceeded. For the HH-like models, an AP was detected based on the m-gate. The m-gate, that is responsible for the Na^+-influx that initiates the AP, needs to cross a threshold value of 0.75 for an AP to be counted. This definition is preferred because the membrane potential oscillates with the carrier frequency, while the m-gate is more robust. An additional rule is set that the m-gate needs to drop below 0.10 before a new AP can be counted, in order to avoid miscounts when the m-gate oscillates around 0.75. To cancel out the influence of transient behaviors caused by the onset of the input current, only a certain time window is considered to determine the FR. This time window is from 100 ms after the stimulation onset until 100 ms + $\frac{20}{f_b}$ after the stimulation onset, where f_b is the beat frequency. In this way, 20 periods of the envelope are included. Then the FR is calculated with:

$$\mathrm{FR} = \frac{N}{t_{\mathrm{window}}} \left(\mathrm{Hz}\right), \tag{18}$$

where N is the number of APs counted and t_{window} is the duration of the stimulation in the investigated time window, being $\frac{20}{f_b}$.

A disadvantage of the FR metric is that it depends on the arbitrary lower and upper excitation threshold values of 0.10 and 0.75. Because it is not ideal that the results depend on the choice of these values, a metric based on the energy of the signal is introduced for extra analysis.In this way it is possible to compare the energy content at the beat and thus the entrainment to the beat frequency. This metric pTI (percentage of TI) is defined as:

$$\mathrm{pTI} = \frac{E_{\mathrm{TI,b}}}{E_{\mathrm{TI,tot}}} \ (-), \tag{19}$$

where $E_{\mathrm{TI,\,b}}$ is the sum of the energy at the beat frequency and the first harmonic of the beat frequency in the frequency spectrum of the membrane potential in response to the TI signal. $E_{\mathrm{TI,\,tot}}$ is the total energy in the membrane response to the TI signal (i.e., the sum of the magnitudes at all frequencies). The total energy is restricted to energies at frequencies higher than 0 Hz in the frequency spectrum. The DC-component is thus not taken into account, to ensure that pTI is independent of the resting potential. Although the energy metric is no direct representation of the activation of the neuron, pTI will increase when the neuron starts firing at the beat frequency and will decrease again when the neurons has more than one AP per beat.

2.5 | Software

The programming, analysis and simulations were performed in MATLAB R2021b. The ode45, ode15s, and ode4 solvers of Matlab were used to calculate the neuronal response numerically (Shampine & Reichelt, 1997). For example, the fixed step ode4-solver was needed for transforming the signals to the frequency spectrum. The variable step variable order solvers, ode45 and ode15s were used to speed up the simulations when no frequency information was needed. The principle of the ode45 and ode15s solvers is explained in Ashino et al. (2000).

3 | RESULTS

A summary of the most important results is given in Tables 3 and 4. Table 3 shows for which of the discussed models it is possible to get a TI zone. The TI zone is defined as the range of input intensities for which the TI signal causes regular firing and the sine input with the same carrier frequency does not cause regular firing. Regular firing is defined as the neuron having more than one spike during the considered time window explained in Section 2.4. Because the first 100 ms are not included in the calculation of the FR, the APs will occur at regular time intervals during the stimulation.

TABLE 3 Summary of the existence of a TI zone for the discussed models.

	Yes	No	Up to which beat frequency?
Leaky integrate-and-fire (LIF)	x		All beat frequencies
Exponential integrate-and-fire (EIF)		x	/
Adaptive and exponential integrate-and-fire (AdEx)		x	
Hodgkin–Huxley (HH)	x		±100 Hz
Frankenhaeuser–Huxley (FH)	x		
Generalized Hodgkin–Huxley (gHH)	x		
Linearized Frankenhaeuser–Huxley (FH1)	x		

Note: EIF includes both the EIF1 and EIF2 model. An estimation is given up to which beat frequency the TI zone would exist. For the Hodgkin–Huxley-like models this is a rough estimation of the order of magnitude as it would differ slightly depending on the model and the carrier frequencies.

TABLE 4 Summary of the gate parameter values, for which there is a TI zone in the FH model with a carrier frequency of 3 kHz and a beat frequency of 100 Hz.

	a (1/mV)	b (mV)	k (–)
m	Whole range (0.12–0.25)	>28	<1.6
h	Whole range (−0.25–−0.1)	<19	Whole range (0.23–4)
n	Whole range (0.05–0.25)	Whole range (0–50)	Whole range (0.1–4)

Note: Whole range indicates that there is a TI zone for the whole investigated range of this parameter.

3.1 | IF models

The aim of this section is to explore whether IF neurons exhibit lower spiking activity in response to a TI signal compared to a sinusoidal signal. Additionally, we aim to determine how the introduction of greater complexity to the model affects this phenomenon. Figure 2 shows the threshold for regular firing, induced by a TI waveform (solid lines) and by a single sinusoid at the same carrier frequency (dashed lines). In the case of the LIF model, the TI signal causes APs at a lower threshold than the sinusoidal signal. The LIF

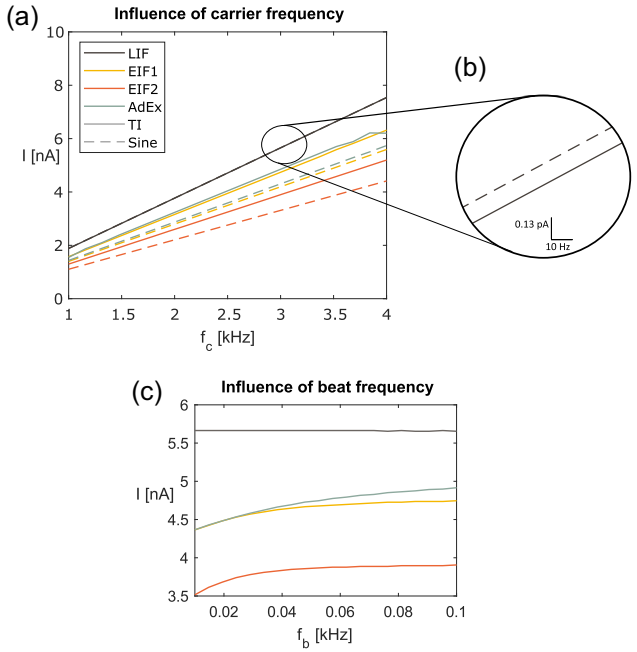

FIGURE 2 Threshold lines for regular firing with a TI input (solid lines) and a sinusoidal signal (dashed lines) in integrate-and-fire (IF) models. The thresholds are shown for the leaky integrate-and-fire (LIF), exponential integrate-and-fire with $\Delta_T = 2$ mV (EIF1), exponential integrate-and-fire with $\Delta_T = 15$ mV (EIF2) and adaptive and exponential integrate-and-fire (AdEx) neuron. (a) Overview of the influence of the carrier frequency on the thresholds all IF models for a beat frequency of 100 Hz. (b) Detail of the LIF model showing a slightly lower threshold for the TI signal. (c) Threshold lines for regular firing with a TI input with a carrier frequency of 3 kHz and a beat frequency f_b.

model thus shows a TI zone. However, the width of this zone is on average only 0.065% of the threshold of the TI signal. For both EIF models, the single sinusoid causes regular firing at a lower threshold than the TI signal. The TI threshold is 1.1 and 1.2 times higher than the sine threshold for the EIF1 and EIF2 model, respectively.

For the AdEx-model, the TI signal again causes firing at higher intensities (approximately 1.1 times higher for a TI signal than for a sinusoidal signal). For all models and all signals, it is clear that for a higher carrier frequency, a higher input is needed to achieve stimulation. None of the IF models showed a depolarization block over the range of 1–4 kHz. This is because sodium and potassium channels are needed to get depolarization block.

3.2 | Effect of nonlinearity in current equations

In this section, the FH1 and gHH models are constructed and compared to the FH and HH models to investigate whether the nonlinearity of the GHK model is of importance to model the neuronal response to TI signals and sinusoidal signals. Two methods are used to determine the Taylor expansion points for the gHH and FH1 models, as described in Section 2.2. For the first method, the expansion points are chosen equal to the Nernst reversal potentials of the ion currents. For the HH-model, this results in $V_{\mathrm{Na},0} = 45$ mV and $V_{\mathrm{K},0} = -82$ mV. For the FH-model this results in $V_{\mathrm{Na},0} = 54$ mV, $V_{\mathrm{K},0} = -98$ mV, and $V_{p,0} = 54$ mV.

For the second method, the average correlations are calculated as described in Section 2.1. The maximum for the FH1v2-model can be found at ($V_{\mathrm{Na},0} = -31$ mV, $V_{\mathrm{K},0} = -37$ mV) and is equal to 0.99. The average correlation for the FH1v1-model is 0.92. For the gHHv2-model, the maximum is at ($V_{\mathrm{Na},0} = 0.34$ mV, $V_{\mathrm{K},0} = -79$ mV) and is equal to 0.971. The average correlation for the gHH1v1-model is 0.79. Supporting Information S1: Figure S1 shows the average correlation as function of the Taylor expansion points for the gHHv2 and FH1v2 models. Some examples of voltage traces are shown in Supporting Information S1: Figure S4.

3.2.1 | FH versus FH1

Figures 3a(i)–(iii) show the energy plot of the FH-model and the difference with the energy of the FH1-models ($\mathrm{pTI}_{\mathrm{FH1}} - \mathrm{pTI}_{\mathrm{FH}}$) as a comparison. In Figure 3a(i) it can be seen that for a higher f_c value, there is a larger range of input intensities for which the neuron reacts at the beat frequency of the TI-input. Also for a higher f_c, a higher input is needed to achieve spiking. Moreover, it can be seen that the behavior of the FH1-models is very similar to the original FH-model (Figures 3a(ii),(iii)). Here, FH1v2 is a closer match than FH1v1 to the original FH-model. The only difference is that the FH1-models get high energies at the beat frequency at higher input intensities.

The plots of the threshold lines can be used to compare the models as well. These results are shown in Figure 3a(iv)–(vi). From the threshold lines, the TI zone can be deduced. Again, it can be seen that the models are very alike with some minor differences (maximal relative difference between thresholds of 15% and 3.5% for FH1v1 and FH1v2 with respect to FH, respectively). Comparing the two solid lines, the FH model and FH1 models have a TI zone in the whole range of the carrier frequency from 1 to 4 kHz. The maximal width of the TI zone is 31, 35, and 30 μA/cm^2 for the FH, FH1v1, and FH1v2 model, respectively. The FH1v2-model again shows the best match to the FH-model over the whole f_c-range. Considering the fact that these TI zones are very small, an example is shown in the supplementary information with a larger TI zone (Supporting Information S1: Figure S5). In this case, the a and b

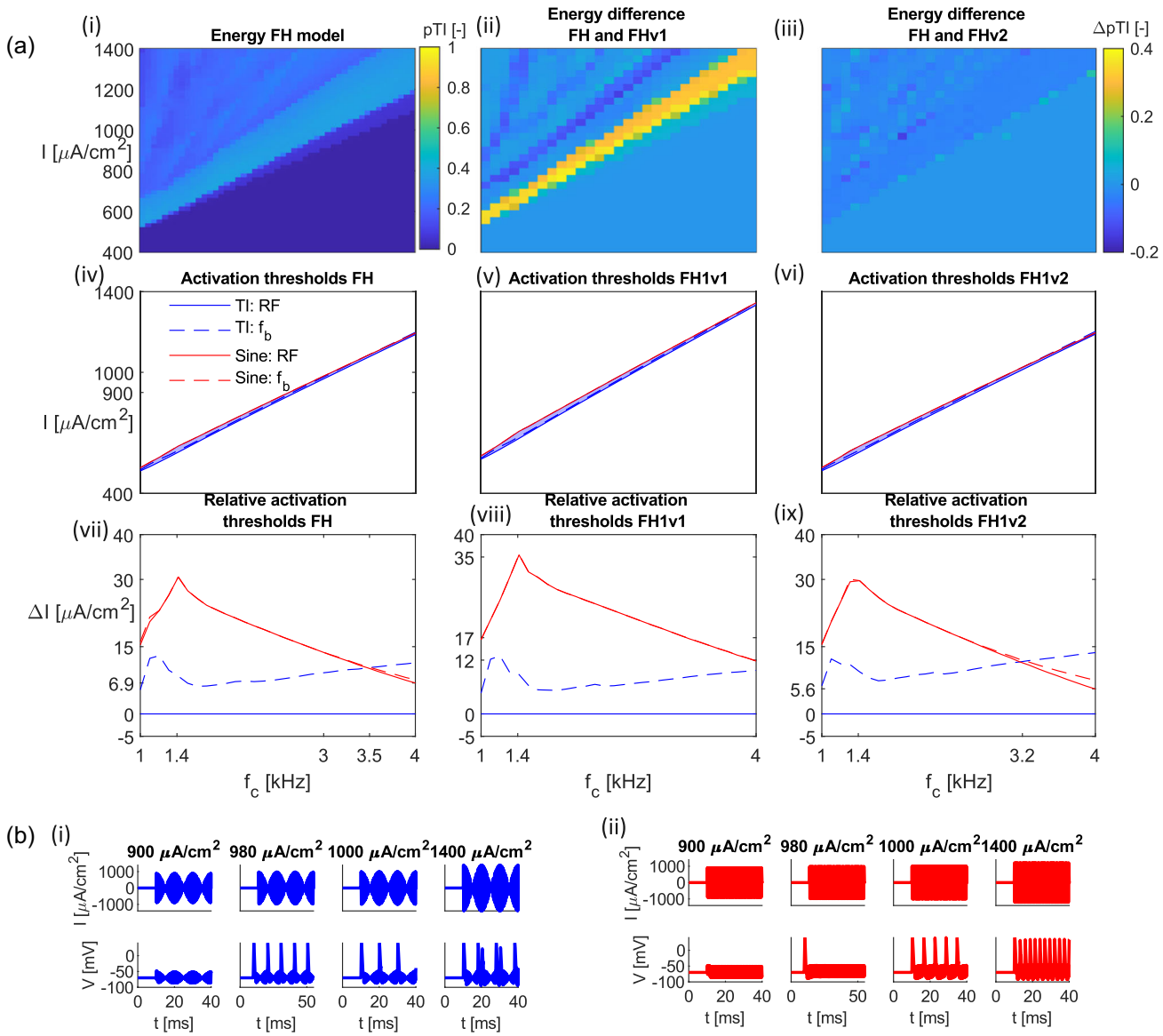

FIGURE 3 (a) Comparison of the Frankenhaeuser–Huxley (FH) and linearized Frankenhaeuser–Huxley (FH1) model for a beat frequency f_b = 100 Hz, showing the qualitative similarity of all models. (i) 2D plot of the energy metric for the FH model. (ii)–(iii) Difference between the energy metric of the FH1v1 and FH1v2 model with respect to the FH model showing a better fit for the FH1v2 model. (iv)–(vi) Absolute threshold lines for TI and sinusoidal stimulation to obtain regular firing (RF) and firing at the beat frequency (f_b) in the FH, FH1v1 and FH1v2 models, respectively. The blue shade indicates the TI zone. (vii)–(ix) Relative threshold lines with respect to the threshold line of regular firing (RF) of the TI-input in the FH, FH1v1 and FH1v2 models, again showing a better fit for the FH1v2 model. (b) Examples of the spiking behavior for TI (i) and sinusoidal (ii) stimulation for beat frequency of 100 Hz and carrier frequency of 3 kHz, showing how the TI signal causes firing at lower thresholds and constrains the APs to the beats.

parameters of the logistic function are changed (cf. Equation 17). The influence of these parameters are discussed in Sections 3.3.2 and 4.4.2.

Moreover, it can be seen that higher intensities are needed to obtain firing at the beat frequency, compared to regular firing. For the FH model the additional intensity needed is 5.4 up to 13 μA/cm^2 in the range of 1–4 kHz. Finally it is interesting to consider the FR for the sine at regular firing. For $f_c > 1.2$ kHz, these FRs are always above 80 Hz. Note that firing at the beat frequency means that one AP occurs within every beat. This does not necessarily have to be the exact same time during a beat, but this is more or less the case around the activation threshold. At higher intensities, when the FR of the neuron becomes higher than the beat frequency, it is possible that the number of APs per beat is more irregular for the TI input. Some cases are shown in Figure 3b(i). For the sinusoidal input (Figure 3b(ii)), the FR increases more linear with the input intensity.

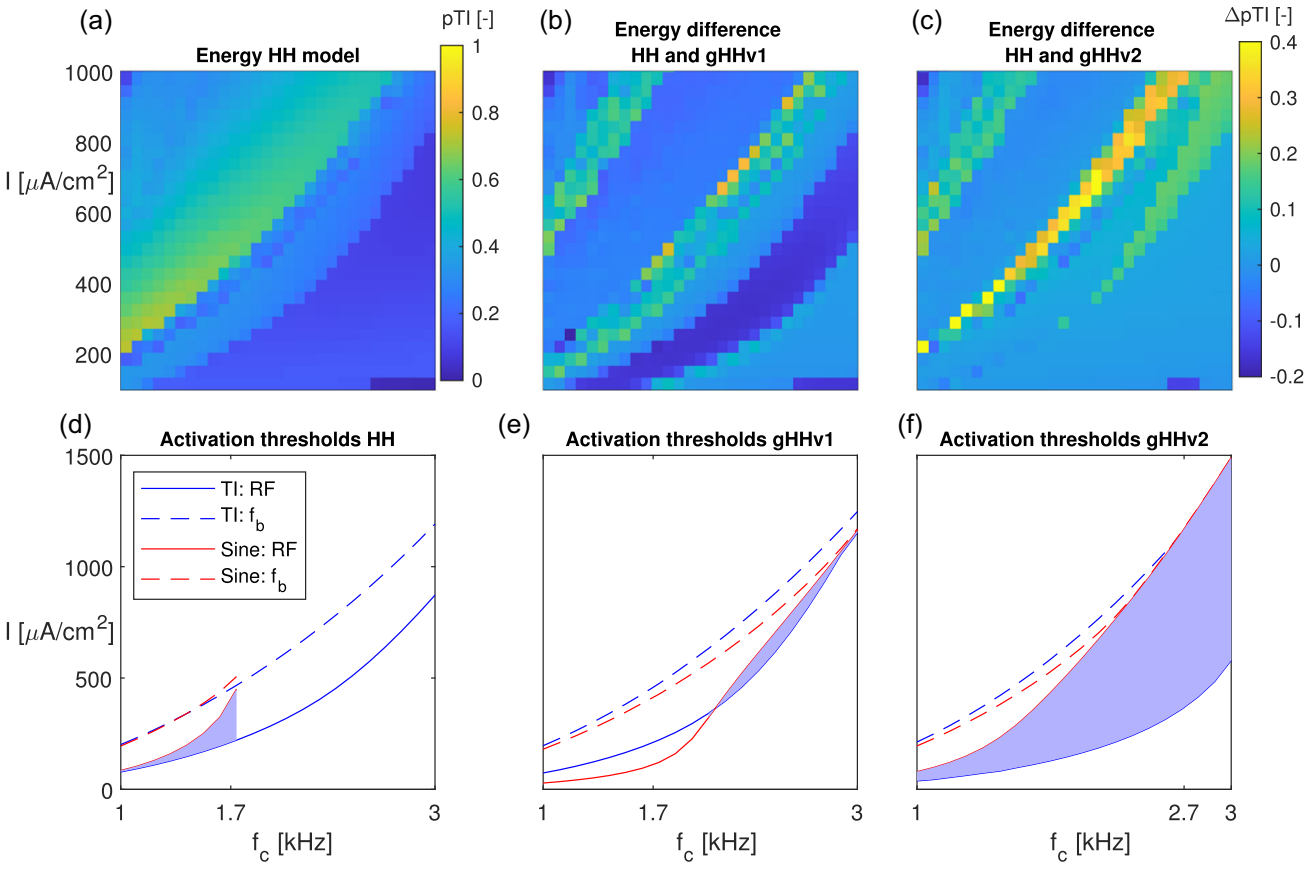

FIGURE 4 Comparison of the Hodgkin–Huxley (HH) and generalized Hodgkin–Huxley (gHH) model for a beat frequency f_b = 100 Hz. (a) 2D plot of the energy metric for the HH model. (b, c) Difference between the energy metric of the gHH1v1 and gHH1v2 model with respect to the HH model, respectively. (d–f) Threshold lines for regular firing (RF) and firing at the beat frequency (f_b) of the HH, gHHv1 and gHHv2 models, respectively. The blue shade indicates the TI zone.

3.2.2 | HH versus gHH

The results for the energy metric and the firing thresholds for the HH and gHH models are shown in Figure 4. From the energy plots it seems that the models again react very similar with only some minor differences due to the approximation. The firing thresholds however suggest that there are big differences for a sinusoidal input. For the sinusoidal input in the HH model, the neuron never spikes above a carrier frequency equal to 1.7 kHz, while for the gHH-model spiking is seen over the whole f_c-range. It is thus possible that the GHK-nonlinearity assures more robustness for quickly oscillating signals. Regarding the TI zone, it is visible that in the whole range in which the pure sine is able to cause APs, the TI signal has a lower threshold. For the gHHv1 model, there is only a TI zone for $f_c > 1.7$ kHz. The gHHv2 model again shows a TI zone over the whole f_c-range between 1 and 3 kHz. The maximal width of the TI zone is 286, 226, and 911 μA/cm^2 for the HH, gHHv1, and gHHv2 model, respectively. Interesting is the threshold for firing at the beat frequency. This threshold of the sinusoidal input is lower than that of the TI input for certain parameter choices. This applies for the HH model for $f_c < 1.4$ kHz, in the whole tested f_c range for the gHHv1 model and for $f_c < 2.6$ kHz for the gHHv2 model.

3.3 | Gates

3.3.1 | Time constants

This section aims to investigate the nonlinearities of the gate characteristics. This portion specifically focuses on the time constants of the ion gates, whereas the next part will focus on the steady state constants of the ion gates. Figure 5a shows the influence on the firing thresholds for the different k-parameters. The range of k-parameters that is reported is the range for which most qualitative changes occur. For the m-gate (Figure 5a(i)), a logarithmic trend is followed. The thresholds increase with increasing k_m-values until it reaches a plateau. Moreover, the blue and red lines cross around $k_m = 1.6$, meaning the TI zone disappears for higher k_m-values.

For very low values of k_h (<0.7) (Figure 5a(ii)), the minimal input intensity needed to achieve spiking

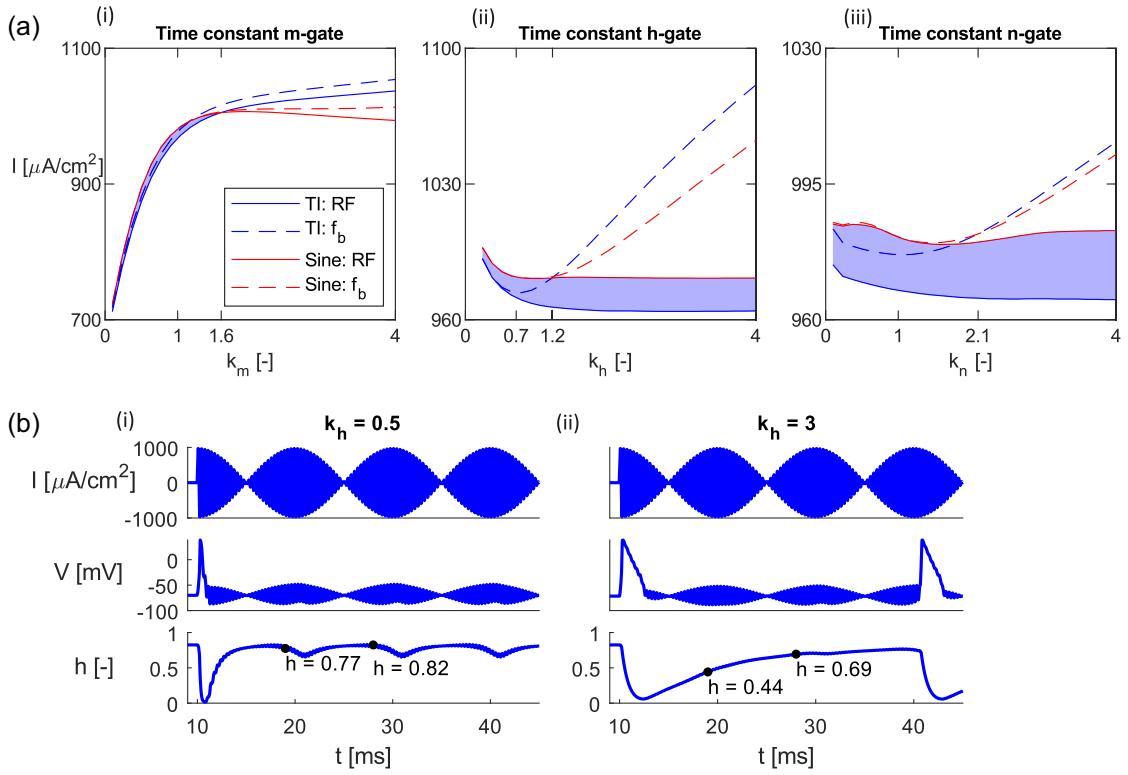

FIGURE 5 (A) Comparison of the threshold lines for regular firing (RF) and firing at the beat frequency f_b = 100 Hz for different k_x-values for the Frankenhaeuser–Huxley (FH) model (f_c = 3 kHz) showing the influence of the time constant on the activation threhsolds. The blue shade indicates the TI zone. (i) m-gate. (ii) h-gate. (iii) n-gate. (b) Examples of the influence of the k_h parameter, showing that spikes can dissappear with both lower and higher k_h, but with different mechanisms.

increases rapidly for both the TI and sine signal for decreasing k_h values. When $k_h < 0.1$, it is not possible anymore to create APs. For $k_h > 0.7$, the threshold lines increase for firing at the beat frequency but stay approximately constant for regular firing.

Similar results are found for the n-gate: for very low k_n-values ($k_n < 1$) (Figure 5a(iii)), all input thresholds increase, while for high k_n-values the thresholds stay more or less constant except for firing at the beat frequency.

Furthermore, it can be seen that the TI signal is able to cause regular firing at lower input intensities than needed for firing at the beat frequency. For low k-values, the solid and dashed blue line in Figure 5 are almost equal. In contrast, a gap of 17, 116, and 41 μA/cm^2 arises for $k_m = 4$, $k_h = 4$, and $k_n = 4$, respectively.

It can again be seen that for certain k values the threshold for firing at the beat frequency is higher for the TI signal than for the sinusoidal signal. This is the case for $k_m > 1.2$, $k_h > 1.2$, and $k_n > 2.1$.

Equation (23) provides more insight into the relation between the optimal beat frequency and the membrane channel dynamics. The optimal beat frequency is the frequency for which a minimal input intensity is needed to achieve firing at the beat frequency. Note that when the intensity is driven up even further then this threshold, neurons can have multiple APs per beat. To derive Equation (23), it is assumed that two phases can be distinguished. In each phase τ_x and x_∞ are constant. In the first phase, the gate characteristics take their values at the membrane potential at the peak of the AP. In the second phase, the gate characteristics take their values at the resting potential. This assumption might not be acceptable for the m-gate, which can be approximated as an instantaneous function $m = m_\infty(V)$ due to its fast nature. A second assumption is that when looking at threshold values, the AP is induced at the top of the beat and the gates should be restored around the node of the TI signal. A third assumption is that x does not change much in the half period before the AP. This means these two phases should be ran through in a half period of the envelope $\left(= \frac{1}{2f_b}\right)$. This assumption is supported by our observation in a simplified HH-model, that the h-gate is opened at the envelope node for beat-locked spiking (Plovie et al., 2022).

The starting point in the derivation is Equation (3). With the assumption of a constant τ_x and x_∞, the solution for x during the first and second phase is shown in Equations (20) and (21), respectively.

$$x(t) = (x_0 - x_{\infty,1})\exp\left(-\frac{t}{\tau_{x,1}}\right) + x_{\infty,1}, \qquad (20)$$

$$x(t) = (x_1 - x_{\infty,2})\exp\left(-\frac{t}{\tau_{x,2}}\right) + x_{\infty,2}. \quad (21)$$

The next step is to solve $x(t_1) = x_1$ for t_1 and $x(t_2) = x_2$ for t_2. The total time is then the sum of t_1 and t_2:

$$\Delta t = t_1 + t_2 = -\tau_{x,1}\ln\left(\frac{x_1 - x_{\infty,1}}{x_0 - x_{\infty,1}}\right) - \tau_{x,2}\ln\left(\frac{x_2 - x_{\infty,2}}{x_1 - x_{\infty,2}}\right), \quad (22)$$

where x can be h or n. Here, x_0, x_1, and x_2 are the gate parameters at the crest, somewhere between crest and trough (at the minimum of the h-gate or the maximum of the n-gate), and at the trough of the envelope, respectively. The optimal beat frequency then becomes:

$$f_{b,opt} = -\frac{1}{2\left(\tau_{x,1}\ln\left(\frac{x_1 - x_{\infty,1}}{x_0 - x_{\infty,1}}\right) + \tau_{x,2}\ln\left(\frac{x_2 - x_{\infty,2}}{x_1 - x_{\infty,2}}\right)\right)}. \quad (23)$$

Because k_x is directly related to the time constant (see Equation 16), a slower gate means that a lower beat frequency is better. This explains the inverse proportionality of the optimal beat frequency with k_x. With this equation, there is an optimal beat frequency for every gate but of course there is only one optimal beat frequency for the whole system. This should be a combination of the different optima for the different gates. Still, Equation (23) gives some mathematical insight into why there is an optimal beat frequency and how it depends on the different gate parameters. As an illustration, when the parameters ($h_0 = 0.75$, $h_1 = 0.025$, $h_2 = 0.75$, $h_{\infty,1} = 0$, $h_{\infty,2} = 0.80$, $n_0 = 0.05$, $n_1 = 0.56$, $n_2 = 0.05$, $n_{\infty,1} = 1$, and $n_{\infty,2} = 0.025$) are applied in Equation (23) in the case of spiking at the beat frequency, the resulting optimal beat frequency is 51 Hz for the h-gate and 119 Hz for the n-gate. From the simulations it was found to be 53 Hz for the whole system. When $k_n = 3$, the optimal beat frequency for the n-gate according to Equation (23) changes to 40 Hz while the optimal beat frequency from the simulations is 46 Hz. For $k_h = 3$, the optimal beat frequency for the h-gate according to Equation (23) changes to 17 Hz while the simulation gives 23 Hz. The optimum is thus inbetween the optimal values of the n-gate and h-gate. The results suggest that the presence and the magnitude of the TI zone depends heavily on the rate at which the ion gates respond as well as the chosen beat frequency.

3.3.2 | Steady-state values

The effect of changing the slope of the m-gate's membrane potential dependency is shown in Figure 6a. A higher a-value shifts the TI zone to higher input currents. The influence of the b-value (i.e., shifting the logistic function along the x-axis) of the m-gate is similar (Figure 6b). A small increase in the b-value makes the threshold lines shift to higher input currents. Moreover, a plateau is observed for $b < 27$ mV where the neuron fires spontaneously.

For the h-gate, a similar but opposite effect is seen. An increase in b-value shifts the thresholds, and thus the TI zone, to lower input currents (Figure 6d). It has to be noted that this effect is less pronounced: For the m-gate, a change in b-parameter from 25 to 45 mV results in a shift from 0 to 1603 μA/cm^2. For the h-gate, changing the b-parameter from −20 to 20 mV results in a shift from 1249 to 935 μA/cm^2. Increasing the a-parameter of the h-gate increases the threshold for spiking activity. In contrast to the m-gate, it increases in a convex way. An interesting observation is that the threshold for the TI input increases faster than for the sine-input with an intersection of the two dashed lines at $a_h = -0.15\ \frac{1}{\text{mV}}$. Also for the b-parameter, an intersection of the dashed blue and red line can be seen at $b_h = 11$ mV.

In case of the n-gate, increasing the a-value shifts the threshold lines to lower input currents. The TI zone spans over the whole a_n and b_n ranges, but there are intersections of the dashed lines for $a_n = 0.18\ \frac{1}{\text{mV}}$ and $b_n = 34$ mV (Figure 6e,f).

The ranges of a and b in Figure 6 is again chosen based on the qualitative changes of the graph. The dependency of the existence of a TI zone on the steady state values and time constants is summarized in Table 4. These results suggest that the TI zone is not only defined by the rate at which the ion gates respond, but also on the state they converge to and thus on all aspects of the nonlinearity introduced by the ion channels.

4 | DISCUSSION

The AdEx model has been used before in Esmaeilpour et al. (2021) to model a hippocampal network. Simpler IF models could be used for the same purpose. The HH-like models primarily focus on modeling the dynamics of the ion channels. From our results it follows that IF models individually can not reproduce a reliable TI zone. In the HH-like models there can be a clear TI zone depending on the exact channel dynamics. The details are discussed below.

4.1 | IF models

Except for the LIF model, for all investigated IF models it was seen that no TI-behavior is present (Figure 2). Although the LIF model does not contain any nonlinearities, it is still possible to get a TI zone,

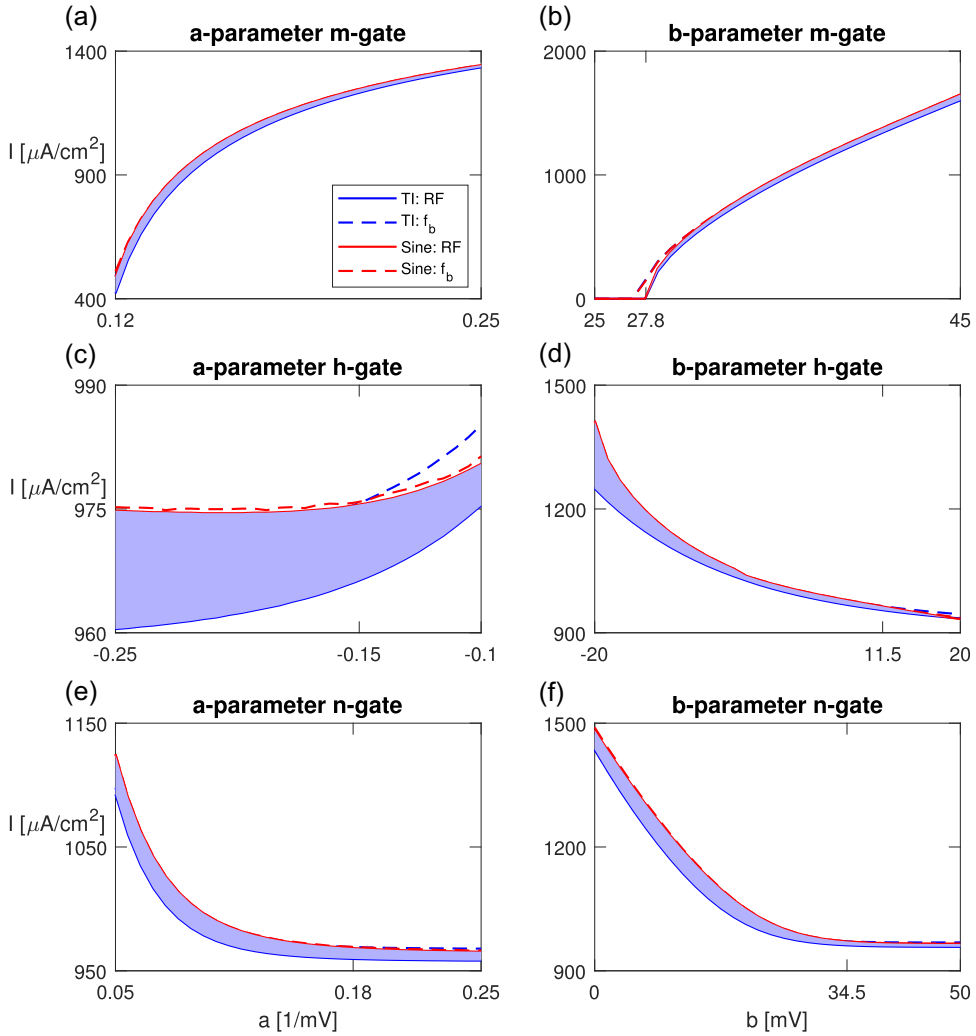

FIGURE 6 Results for the threshold lines for the Frankenhaeuser–Huxley (FH) model with x_∞ as a logistic function with a varying a-parameter and constant b-parameter (left) and a varying b-parameter and constant a-parameter (right) with $f_c = 3$ kHz and $f_b = 100$ Hz. This figure shows the influence of the steady state values of the gate parameters on the activation thresholds. The blue shade indicates the TI zone. (a, b) m-gate. (c, d) h-gate. (e,f) n-gate.

despite being small. The reason for this is that the TI signal contains both the f_1 and f_2 frequencies, while the sine only contains the f_c frequency. Because $f_1 < f_c$, the threshold is slightly lower for the TI signal than for the pure sinusoid. This is further explained with the analytical result in the supplementary information (Section S2). From the transition from LIF to EIF it is clear that adding a nonlinearity makes the TI zone disappear. The transition from EIF to AdEx did not show major differences. However, in Esmaeilpour et al. (2021), AdEx neurons did show correspondence with the experiments of Grossman et al. (2017). In that study, they used a network of neurons rather than a single neuron. They also state that the effect was probably seen because they added the slow $GABA_b$ channels to the network, while isolated AdEx neurons are unlikely to exhibit the TI behavior.

4.2 | FH and HH

Two conclusions can already be drawn from the FH and HH models. First, the threshold for the neuron to exhibit regular firing or to fire at the beat frequency is not equal. Second, the FR for a sinusoidal input is around 100 Hz in most cases. The reason for the first conclusion will be discussed more in depth in the next sections. The second conclusion points out the importance of TI stimulation. When applying a TI input, it much easier to control the FR of the neurons than for a sinusoidal input, for which the FR changes much faster with the input intensity. For pure sines, lower FRs can then only be reached when the current is applied in a pulsed way. If indeed the difference between the excitation thresholds of a TI signal and a sinusoidal signal is very small, the controllability of the FR with the TI signal can still be an advantage for TI stimulation as in

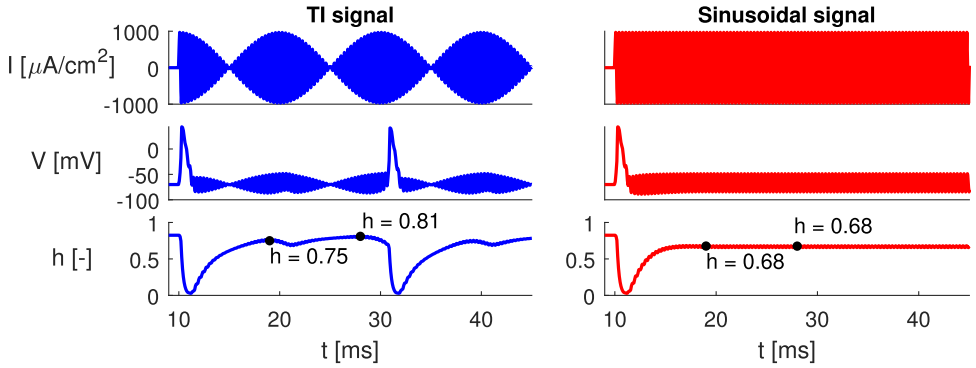

FIGURE 7 Illustration of the different responses of an Frankenhaeuser–Huxley (FH) neuron to a temporal interference (TI) signal (f_b = 100 Hz, f_c = 3 kHz and I_e = 970μA/cm^2) and a sinusoidal signal (f = 3 kHz and I_e = 970μA/cm^2). (a) TI-input eliciting an AP every other beat. The state of the h-gate and n-gate (indicated in blue) at two consecutive beats show the need for the recovery of the gate to elicit an AP. (b) Sinusoidal input having only an AP at the stimulus onset. The state of the h-gate and n-gate show that the gates do not change besides oscillations because of the continuous sinusoidal input.

Howell and McIntyre (2021) and Wessel et al. (2022), where it is proposed to use a subthreshold TI signal. As previously noted, some of the TI zones seem rather small. While this could be because of the gate characteristics of this model, it might also be possible that network effects increase the robustness to the application of TI stimulation. However, this remains uncertain. Some studies as Esmaeilpour et al. (2021), Luff, Peach, et al. (2024), and Martinez et al. (2023) do show the importance of network effects.

4.3 | Importance of the GHK nonlinearity

From the comparison between the FH and FH1 models it became clear that linearizing the GHK-equation of the ion currents has a minor effect on the neuronal response. However, the TI zone does not disappear as seen with the IF-models. Instead, the TI zone behaves as an approximation of the more complex model without losing its most important characteristics. Simply adding a nonlinearity in the differential equation of the membrane potential is thus not sufficient to fully change the behavior of the neuron model. The shift of the pTI-metric to higher input intensities is explained by the observation that the Na^+-current is lower in magnitude for the FH1-models, so a higher input is needed to achieve firing. This is supported by the fact that the FH1v2-model is a better approximation in which the magnitude of the Na^+-current is higher, especially at lower membrane potentials.

The comparison of the HH and gHH models shows larger differences. For example, it is less straightforward to determine which linearized model better approximates the behavior of the HH-model. However, with both models it is possible to achieve a TI zone. From this it can be concluded that the GHK nonlinearity is not the main reason for a neuron model to show a TI zone.

4.4 | Gate nonlinearities contribute to underlying mechanism

The effect of the different characteristics of the gates will be explained in this section, but the mechanism of TI can be best explained with Figure 7. Figure 7 shows that a TI signal can elicit an AP at every other beat, while the sinusoidal signal with the same carrier frequency can only elicit an AP at the stimulation onset. An explanation for this behavior can be found by examining the gates. For the response to a sinusoidal signal, all the gates reach a state of small-amplitude oscillations about a quasi-equilibrium value (h = 0.68). However, the values around which they oscillate are not favorable for neuronal excitation (a higher h-value and a lower n-value would be better). Comparing this to the TI signal (Figure 7), it can be seen that because this input signal drops to lower values for a longer period, the n- and h- gates are able to return to values that are more favorable to create an AP. This is further illustrated by the observation that no AP is induced by the second beat in, because the h-gate value is still too low (h = 0.75). However, at the subsequent beat, further opening of the h-gate (h = 0.81) results in an AP.

4.4.1 | Time constants

The results in Figure 5a(i) show that the m-gate time constant has the most influence on the behavior of the neuron. For lower time constants, the neuron starts to fire at lower amplitudes of the input current. This can be explained by the fact that the fast reaction of the m-gate is responsible for the initiation of an AP. If the

m-gate would react infinitely fast, an AP would be created at the moment that a certain threshold of the membrane potential is reached. When the m-gate reacts with a certain lag, a higher membrane potential should be reached to create an AP, as the m-gate needs some time to get to a value that is high enough to push the membrane potential into an AP. However, if the potential starts decreasing again shortly after its maximum is reached and the m-gate starts decreasing as well, no AP will be created. Because of this, the firing thresholds increase proportional to the m-gate time constant (cf. Figure 5a(i)). Above $k_m = 1$, the threshold for regular firing of the sine decreases slightly. This is due to an interplay of the closing and opening of the m-gate over multiple periods of the sine.

For the h-gate it was seen that both very low and very high time constants increase the threshold current for firing at the beat frequency (Figure 5b). In the case of a very low time constant, this is because the h-gate closes too fast (Figure 5b(i)). In contrast, high time constants result in reduced h-gate opening after a first AP, resulting in higher excitation thresholds (Figure 5b (ii)). This also explains why from a certain point (around $k_h = 1.8$), increasing k_h only has an influence on the threshold for firing at beat frequency of the TI signal (dashed blue line). The slower the h-gate reacts, the more beats are skipped and the higher the input current has to be to force the neuron to respond to every beat. This will not affect the regular firing threshold of the TI signal because the effect is only on the time between spikes. When the h-gate has reopened, the rapid response of the m-gate will always be able to initiate a new AP, only the FR will be lower. For sine-input, the same reasoning can be made: waiting long enough for the h-gate to reopen will always lead to a new AP, only with a lower FR.

The reasoning for the n-gate is very similar to that of the h-gate. Opening of the n-gates causes an outflow of K^+-ions resulting in a decrease of the membrane potential. Both gates can thus counteract the formation of an AP with the only difference that the effect of the h-gate is present in the form of a multiplication with the m-gate, while the effect of the n-gate is present in the addition of the K^+-current. Therefore, a fast-reacting n-gate (low k_n) makes it harder to create an AP and thus a higher input current is needed to achieve spiking (cf. Figure 5a(iii)). For a slower n-gate (high k_n), the K^+-outflow will still be too high to initiate a new AP at the next beats. The reasoning why the threshold for firing at the beat frequency of the TI signal changes most with increasing k_n is the same as with increasing k_h.

The threshold for firing at the beat frequency is lower for a sine input than for a TI input for $k_m > 1.2$, $k_h > 1.2$, or $k_n > 2.1$. This is because increasing the input intensity above the threshold for spiking for a sine will increase the FR in a continuous way. In contrast, increasing the intensity above the threshold for a TI signal will not immediately increase the FR. The FR will only increase when more beats can cause an AP. Therefore, the FR will make a discrete jump when increasing the input intensity. Moreover, at the threshold, the neuron is expected to fire around the trough of the envelope. When the input is just too low, it is possible that some beats do not elicit an AP, because the states of the gates were not right in the short time frame around the top of the beat. In this way, it is possible that the sine causes firing at the beat frequency of the TI signal it is compared to, but the TI signal needs a higher intensity to fire at its beat frequency. It should be noted that in experimental studies as Grossman et al. (2017) and Gomez-Tames et al. (2021), the beat frequency did not seem to have such a big influence, while it did in Budde et al. (2023). This might be because of different reasons. It could for example have to do with neurons in each other's neighborhood having slightly different properties and thus a slightly different minimum. Moreover, these neurons could be interconnected, causing the minimum to be less prominent.

4.4.2 | Steady-state values

From the discussion above, it has become clear that the values of the gates play an important role. The time constants that were discussed play a role in how fast the gates can reach a certain value. The steady-state characteristic then determines to which value the gates evolve. This is investigated in this study by changing the a- and b-parameters in the logistic function approximation of the gates.

Starting with the m-gate (Figure 6a,b), a TI zone is present for all the investigated a-values. Increasing the steady-state values shifts the TI zone to higher input currents. For a higher b-value, a TI zone appears, while for the a-value, the TI zone becomes smaller. The reason for the shift of the threshold to higher input currents is that for higher a- or b-values, the m-gate is in a more closed state at lower membrane potentials. Interestingly, for values of $b < 27$ mV, the neuron fires spontaneously. In other words, the open probability of the m-gate is high enough at low membrane potentials so the neuron can always enter the positive feedback loop to form an AP.

For the h-gate, the behavior for different values of a and b can be explained by the fact that for higher a-values or lower b-values, the h-value around the resting potential is lower. The h-gate is thus already in a more closed state resulting in a lower Na^+-current and a higher input current needed to cause firing.

Useful for the application of TI stimulation is that the steepness of the threshold is not the same for the TI-input and the sinusoidal input. For low b_h-values,

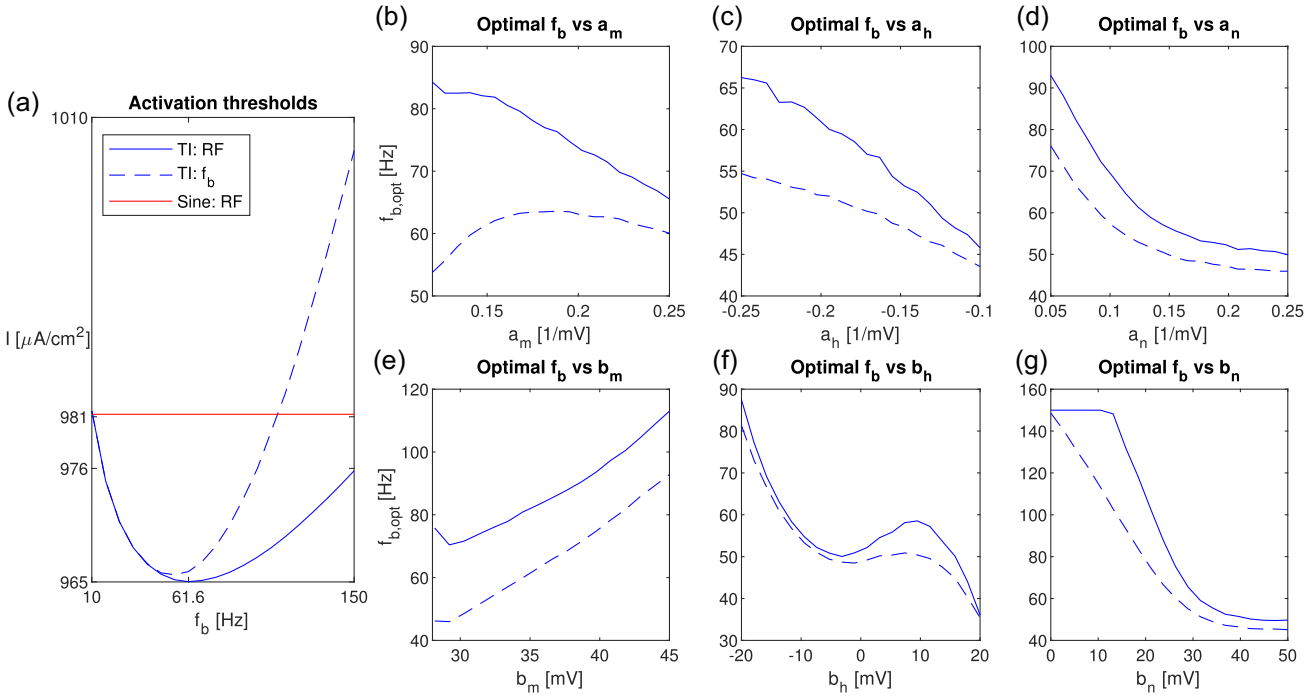

FIGURE 8 (a) Illustration of the threshold-beat frequency relation for regular firing (solid line) and firing at the beat frequency (dashed line) for the Frankenhaeuser–Huxley (FH) model with f_c = 3 kHz, indicating an optimal beat frequency (i.e., a beat frequency for which minimal input current is needed to cause spiking). The threshold for regular firing with a sinusoidal input shows the varying width of the TI zone depending on the beat frequency. (b–g) Minimal beat frequency for different values of the a and b parameters, where the steady state value of a single gate (x = m, h, or n) is substituted by a logistic function. The optimum was found through curve fitting of a fourth order polynomial on the minimum of the simulation and its three closest neighboring datapoints on each side.

this causes a substantial TI zone. The reason for this is the following. When the threshold input is plotted with respect to the beat frequency (Figure 8), it can be seen that a global minimum exists and thus there is an optimal beat frequency for TI stimulation. When the characteristic parameters a, b, and k of the gates are altered, the minimum shifts to other beat frequencies. The beat frequency at the minimal threshold current is shown in Figure 8b–g. For example, increasing the a_h- and b_h-parameter generally shifts the optimal beat frequencies to lower values, with a local maximum at b_h = 10 mV. Hence, the optimal f_b comes closer to 0 Hz and goes further from the case of f_b = 100 Hz with increasing a_h-value. Because the TI signal approximates a sine for $f_b \to 0$ Hz, a sine can be seen as a TI signal with f_b = 0 Hz, with increasing a_h-value, the threshold for a sine increases less steep than the threshold for the TI signal (Figure 6c). The same holds for the increasing b_h parameter in Figure 6d. In this case, the decrease of the red lines is steeper because the sine comes closer to the optimal beat frequency with increasing b_h. On the other hand, the h-value at low membrane potentials increases which is in turn more favorable to create an AP. This means that there is a double effect for the decreasing threshold. For the 100 Hz beat frequency TI-input, the increase in h-value at low membrane potentials for increasing b_h-value again causes a decrease in threshold but because the optimal beat frequency shifts to lower values, the decrease in threshold is less steep. A graphical summary of this mechanism is shown in Figure 9.

Similarly, the dependency if the optimal f_b on a_X and b_X explains the difference in steepness of the thresholds for the sine and the TI signal for the m- and h-gate. The reasoning can also be followed for the k-values. In this case, the effect can be best seen for higher k-values in Figure 5: the gap between regular firing and firing at the beat frequency increases with k which means that the optimal beat frequency is inversely proportional with k.

The reason for the existence of an optimal beat frequency is because of the following. When the beat frequency is too high, some of the gates might not be restored to a value that is sufficient to create a new AP. Because of this, some beats might be skipped in the neuronal response to the TI waveform. When the beat frequency is too low, the TI waveform envelope builds up too slow. Because of this slow build-up, the h-gate tends to close too fast while the n-gate opens too fast. Because of this the input current needed to create an AP is higher. The existence of the optimal beat frequency is in line with the concept of resonance in neurons found by Hutcheon and Yarom (2000). This

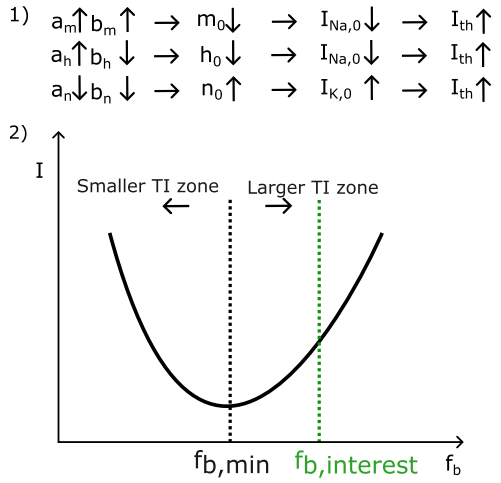

FIGURE 9 Illustration of the influence of the steady state values on the TI zone. (1) This is a schematic of how the a and b parameters influence the magnitude of the activation threshold. (2) This shows that if the optimal beat frequency ($f_{b,\min}$) moves further away from the beat frequency of interest and closer to 0 Hz, the width of the TI zone will be smaller and if the optimal beat frequency moves closer to the beat frequency of the TI signal ($f_{b,\text{interest}}$) and away from 0 Hz, the width of the TI zone will be larger. If the optimal beat frequency moves away from both 0 Hz and the beat frequency of interest, the width of the TI zone depends on the exact shape of I_{th} as a function of f_b.

discussion shows that the resonant beat frequency does not only depend on the time constant of the gates, but also on their steady-state characteristics.

4.5 | Strengths, limitations, and future work

The first strength of this study is the insight that the GHK nonlinearity may not be indispensable for accurately modeling of neuron behavior in response to TI stimulation. An Ohmic approximation can still be of good use. Second, the study further uncovers the critical role of the nonlinear behavior of the ion gates. The fact that an individual neuron responds to a TI signal at lower activation thresholds than a pure sine is highly affected by the ion gates. Not only the time constant of the ion gates is of importance, but also its steady state constants significantly determine the neuron responses. This implicates the importance to account for neuron-specific responses in future research of TI stimulation. Moreover it gives an interesting perspective for future research in more complex neuron models. This study used a more simple model that gives the opportunity to do an extensive parameter study while keeping a good interpretability. These insights can be taken into account when studying and trying to comprehend more complex neuron models.

A first limitation of this study of the underlying mechanism of TI stimulation is that both the spatial properties of the electric field (i.e., both the vectorial nature of the field that leads to elliptical polarization states interacting with morphology extended neurons, and the spatial exposure heterogeneity that could modulate neural activity through an activating function-like mechanism) are not taken into account in the cell models. Other authors have used morphologically correct neuron models, to investigate the neuronal response to TI modulation (Wang et al., 2023). Although morphology is an important factor for TI stimulation, this study focuses on the hypothesis that TI stimulation is predominantly explained by ion channel nonlinearities and timescales. Nevertheless, morphologically realistic models are interesting to obtain quantitative insights into the activation and conduction block thresholds. Moreover, a limitation of point neurons is that it is not always certain if the detected APs can propagate. Additionally, the exact combination of ion channels in the neuron can have an influence as well. A second limitation of this study, is that the TI-modulated point neurons are isolated, while neuronal network simulations have demonstrated the importance of network adaptation (Esmaeilpour et al., 2021).

As future work, it would be interesting to investigate the influence of synaptic time constants on the TI zone. This would be interesting in order to see how much of the effect of a single neuron is carried on to the postsynaptic neurons and by extension an entire neuronal network. The underlying mechanism of TI stimulation can thus be found in a lot of aspects of the neural system and may be a combined effect of several factors. Furthermore, there is a phenomenon called the superexcitable phase of membrane recovery. This holds that after a period of refraction, a period follows where neurons are more excitable (Bostock et al., 2005; Raymond, 1979). It might be worth it to consider this effect in the research to the mechanism of TI stimulation as it might influence the neuron response. Additionally, the influence of changes in resting potentials and reversal potentials can be investigated. Therefore, the investigation in this study of the nonlinearities and time constants in point neurons is a first step in the direction of a comprehensive understanding of neuromodulation by TI.

5 | CONCLUSION

This study consists of two major parts. First, the discussion of the complexity of neuron models needed to be able to model the experimentally observed responses to TI-DBS. Second, the time dynamics of the ion gates in relation to TI stimulation.

From the first part, it can be concluded that the nonlinearity in the GHK-equation alone is not able to explain the underlying mechanism of TI-DBS. For the FH-model, the linearisation causes minor differences in

the neuronal response, that are not sufficient to describe the TI underlying mechanism. For the HH-model, the differences caused by the GHK nonlinearity are larger. However, the HH TI zone is actually larger in the linearized model, confirming that the GHK nonlinearity is not necessary in order to observe neuronal sensitivity to a beating sine. It should be noted that the choice of the expansion points has a big influence on the neuronal behavior as well. From the investigation of the IF-models it can also be concluded that the introduction of a nonlinear term in the differential equations is not able to shift the threshold of the TI-input beneath that of the sinusoidal input.

From the second part, it can be concluded that the nonlinearities intrinsic to the gating dynamics have a large influence on how the neurons react to the TI and sine input. The mechanism is a complex interplay between the gates that is driven by the gate characteristics in terms of the time constants and steady-state values. This paper showed that changing the gates' opening and closing rates can influence the existence and the width of the TI zone. A TI zone can appear with increasing b_m values or with a decrease of the k_m, a_m, or b_h parameter. It was also shown that for a certain neuron, it is possible to find the optimal stimulation parameters to increase the TI zone. This is an interesting finding that is potentially relevant for the optimization of TI stimulation of combinations of different neuronal types at different locations.

ACKNOWLEDGMENTS

We want to thank Michiel De Kesel for the exploratory work and discovering the possible importance of the nonlinearity of the GHK-equation. This research was funded by the FWO-project G019121N. T Tarnaud is a postdoctoral Fellow of the FWO-V (1230222N, Research Foundation Flanders, Belgium). R Schoeters is a Ph.D. Fellow of the FWO-V (11E4520N, Research Foundation Flanders, Belgium).

CONFLICT OF INTEREST STATEMENT

The authors declare no conflict of interest.

DATA AVAILABILITY STATEMENT

The data from this study are available from the corresponding author upon request.

ETHICS STATEMENT

Not applicable.

ORCID

Tom Plovie http://orcid.org/0000-0001-9307-1702
Wout Joseph http://orcid.org/0000-0002-8807-0673

REFERENCES

Acerbo, E., Jegou, A., Luff, C., Dzialecka, P., Botzanowski, B., Missey, F., Ngom, I., Lagarde, S., Bartolomei, F., Cassara, A., Neufeld, E., Jirsa, V., Carron, R., Grossman, N., Williamson, A.: Focal non-invasive deep-brain stimulation with temporal interference for the suppression of epileptic biomarkers. Front. Neurosci. 16, 945221, 2022

Ashino, R., Nagase, M., Vaillancourt, R.: Behind and beyond the matlab ode suite. Comput. Math. Appl. 40, 491–512 (2000). www.elsevier.nl/locate/camwa

Aum, D. J., Tierney, T. S.: Deep brain stimulation: foundations and future trends. Front. Biosci. 23, 162–182 (2018).

Bostock, H., Lin, C. S. Y., Howells, J., Trevillion, L., Jankelowitz, S., Burke, D.: After-effects of near-threshold stimulation in single human motor axons. J. Physiol. 564(3), 931–940 (2005).

Brette, R., Gerstner, W.: Adaptive exponential integrate-and-fire model as an effective description of neuronal activity. J. Neurophysiol. 94, 3637–3642 (2005).

Budde, R. B., Williams, M. T., Irazoqui, P. P.: Temporal interference current stimulation in peripheral nerves is not driven by envelope extraction. J. Neural Eng. 20(2), 026041 (2023).

Cao, J., Doiron, B., Goswami, C., Grover, P.: The mechanics of temporal interference stimulation. BioRxiv pp. 2020–04 (2020).

Cao, J., Grover, P.: Do single neuron models exhibit temporal interference stimulation? In: 2018 IEEE Biomedical Circuits and Systems Conference, BioCAS 2018—Proceedings (2018).

Cassarà, A. M., Newton, T. H., Zhuang, K., Regel, S. J., Achermann, P., Kuster, N., Neufeld, E.: Safety recommendations for temporal interference stimulation in the brain. bioRxiv pp. 2022–12 (2022).

Esmaeilpour, Z., Kronberg, G., Reato, D., Parra, L. C., Bikson, M.: Temporal interference stimulation targets deep brain regions by modulating neural oscillations. Brain Stimul. 14, 55–65 (2021).

Frankenhaeuser, B., Huxley, A. F.: The action potential in the myelinated nerve fibre of xenopus laevis as computed on the basis of voltage clamp data. J. Physiol. 171, 302–315 (1964).

Gomez-Tames, J., Asai, A., Hirata, A.: Multiscale computational model reveals nerve response in a mouse model for temporal interference brain stimulation. Front. Neurosci. 15, 684465, (2021).

Grossman, N., Bono, D., Dedic, N., Kodandaramaiah, S. B., Rudenko, A., Suk, H. J., Cassara, A. M., Neufeld, E., Kuster, N., Tsai, L. H., Pascual-Leone, A., Boyden, E. S.: Noninvasive deep brain stimulation via temporally interfering electric fields. Cell 169, 1029–1041 (2017).

Grossman, N., Okun, M. S., Boyden, E. S.: Translating temporal interference brain stimulation to treat neurological and psychiatric conditions. JAMA Neurol. 75, 1307–1308 (2018).

Hodgkin, A. L., Huxley, A. F.: A quantitative description of membrane current and its application to conduction and excitation in nerve. J. Physiol. 117, 500–544 (1952).

Howell, B., McIntyre, C. C.: Feasibility of interferential and pulsed transcranial electrical stimulation for neuromodulation at the human scale. Neuromodulation 24, 843–853 (2021).

Huang, Y., Huang, Y., Datta, A., Parra, L. C.: Optimization of interferential stimulation of the human brain with electrode arrays. J. Neural Eng. 17, 036023 (2020).

Huang, Y., Parra, L. C.: Can transcranial electric stimulation with multiple electrodes reach deep targets? Brain Stimul. 12, 30–40 (2019).

Hutcheon, B., Yarom, Y.: Resonance, oscillation and the intrinsic frequency preferences of neurons. Trends Neurosci. 23(5), 216–222 (2000).

Iacono, M. I., Neufeld, E., Akinnagbe, E., Bower, K., Wolf, J., Vogiatzis Oikonomidis, I., Sharma, D., Lloyd, B., Wilm, B. J., Wyss, M., et al.: MIDA: a multimodal imaging-based detailed anatomical model of the human head and neck. PLoS One 10(4), e0124126 (2015).

Khalifa, A., Abrishami, S. M., Zaeimbashi, M., Tang, A. D., Coughlin, B., Rodger, J., Sun, N. X., Cash, S. S.: Magnetic temporal interference for noninvasive and focal brain stimulation. J. Neural Eng. 20(1), 016002 (2023).

Lee, S., Park, J., Choi, D. S., Lim, S., Kwak, Y., Jang, D. P., Kim, D. H., Ji, H. B., Choy, Y. B., Im, C. H.: Feasibility of epidural temporal interference stimulation for minimally invasive electrical deep brain stimulation: Simulation and phantom experimental studies. J. Neural Eng. 19, 056003 (2022).

Luff, C. E., Dzialecka, P., Acerbo, E., Williamson, A., Grossman, N.: Pulse-width modulated temporal interference (pwm-ti) brain stimulation. Brain Stimul. 17(1), 92–103 (2024).

Luff, C. E., Peach, R., Mallas, E. J., Rhodes, E., Laumann, F., Boyden, E. S., Sharp, D. J., Barahona, M., Grossman, N.: The neuron mixer and its impact on human brain dynamics. Cell Rep. 43, 114274 (2024).

Martinez, S. C., Goswami, C., Forssell, M., Cao, J., Barth, A., Grover, P.: Cell-specific effects of temporal interference stimulation on cortical function (2023).

Mirzakhalili, E., Barra, B., Capogrosso, M., Lempka, S. F.: Biophysics of temporal interference stimulation. Cell Syst. 11, 557–572 (2020).

Missey, F., Rusina, E., Acerbo, E., Botzanowski, B., Trébuchon, A., Bartolomei, F., Jirsa, V., Carron, R., Williamson, A.: Orientation of temporal interference for non-invasive deep brain stimulation in epilepsy. Front. Neurosci. 15, 633988 (2021).

Piao, Y., Ma, R., Weng, Y., Fan, C., Xia, X., Zhang, W., Zeng, G. Q., Wang, Y., Lu, Z., Cui, J., et al.: Safety evaluation of employing temporal interference transcranial alternating current stimulation in human studies. Brain Sci. 12(9), 1194 (2022).

Plovie, T., Schoeters, R., Tarnaud, T., Martens, L., Joseph, W., Tanghe, E.: Influence of temporal interference stimulation parameters on point neuron excitability. In: Proceedings of the Annual International Conference of the IEEE Engineering in Medicine and Biology Society, EMBS, 2365–2368 (2022).

Rampersad, S., Roig-Solvas, B., Yarossi, M., Kulkarni, P. P., Santarnecchi, E., Dorval, A. D., Brooks, D. H.: Prospects for transcranial temporal interference stimulation in humans: A computational study. NeuroImage 202, 116124 (2019).

Raymond, S.: Effects of nerve impulses on threshold of frog sciatic nerve fibres. J. Physiol. 290(2), 273–303 (1979).

Shampine, L. F., Reichelt, M. W.: The matlab ode suite. SIAM J. Scient. Comput. 18(1), 1–22 (1997).

Song, S., Zhang, J., Tian, Y., Wang, L., Wei, P.: Temporal interference stimulation regulates eye movements and neural activity in the mice superior colliculus. In: 2021 43rd Annual International Conference of the IEEE Engineering in Medicine & Biology Society (EMBC), pp. 6231–6234. IEEE (2021).

Sorkhabi, M. M., Wendt, K., Denison, T.: Temporally interfering tms: Focal and dynamic stimulation location. Proceedings of the Annual International Conference of the IEEE Engineering in Medicine and Biology Society, EMBS 2020, 3537–3543 (2020).

Su, X., Guo, J., Zhou, M., Chen, J., Li, L., Chen, Y., Sui, X., Li, H., Chai, X.: Computational modeling of spatially selective retinal stimulation with temporally interfering electric fields. IEEE Trans. Neural Syst. Rehab. Eng. 29, 418–428 (2021).

Sunshine, M. D., Cassarà, A. M., Neufeld, E., Grossman, N., Mareci, T. H., Otto, K. J., Boyden, E. S., Fuller, D. D.: Restoration of breathing after opioid overdose and spinal cord injury using temporal interference stimulation. Commun. Biol. 4, 107 (2021).

Vassiliadis, P., Beanato, E., Popa, T., Windel, F., Morishita, T., Neufeld, E., Duque, J., Derosiere, G., Wessel, M. J., Hummel, F. C.: Non-invasive stimulation of the human striatum disrupts reinforcement learning of motor skills. Nat Hum Behav. 1–18 (2024).

Violante, I. R., Alania, K., Cassarà, A. M., Neufeld, E., Acerbo, E., Carron, R., Williamson, A., Kurtin, D. L., Rhodes, E., Hampshire, A., et al.: Non-invasive temporal interference electrical stimulation of the human hippocampus. Nat Neurosci. 26, 1994–2004 (2022).

von Conta, J., Kasten, F. H., Ćurčić Blake, B., Aleman, A., Thielscher, A., Herrmann, C.S.: Interindividual variability of electric fields during transcranial temporal interference stimulation (ttis). Scientific Reports 11, 20357 (2021).

Wang, B., Aberra, A. S., Grill, W. M., Peterchev, A. V.: Responses of model cortical neurons to temporal interference stimulation and related transcranial alternating current stimulation modalities. J. Neural Eng. 19(6), 066047 (2023).

Wessel, M. J., Beanato, E., Popa, T., Windel, F., Vassiliadis, P., Menoud, P., Beliaeva, V., Violante, I. R., Abderrahmane, H., Dzialecka, P., et al.: Ltp-like noninvasive striatal brain stimulation enhances striatal activity and motor skill learning in humans. bioRxiv pp. 2022–10 (2022).

Xin, Z., Kuwahata, A., Liu, S., Sekino, M.: Magnetically induced temporal interference for focal and deep-brain stimulation. Front. Human Neurosci. 15, 693207 (2021).

AUTHOR BIOGRAPHY

Tom Plovie is a PhD candidate at the faculty of engineering and architecture of Ghent University. He has a BSc degree in Engineering Physics and an MSc degree in Biomedical Engineering. He work for the department of Information Technology.

SUPPORTING INFORMATION

Additional supporting information can be found online in the Supporting Information section at the end of this article.

How to cite this article: Plovie T, Schoeters R, Tarnaud T, Joseph W, Tanghe E: Nonlinearities and timescales in neural models of temporal interference stimulation. Bioelectromagnetics, 46, e22522 (2025)